



# Influence of corrosion on the electrical and mechanical performance of hybrid busbars



Rui F.V. Sampaio <sup>a</sup>, João P.M. Pragana <sup>a</sup>, Ivo M.F. Bragança <sup>b</sup>, Carlos M.A. Silva <sup>a</sup>,  
João C.S. Fernandes <sup>c</sup>, Paulo A.F. Martins <sup>a,\*</sup>

<sup>a</sup> IDMEC, Instituto Superior Técnico, Universidade de Lisboa, Portugal

<sup>b</sup> CIMOSM, Instituto Superior de Engenharia de Lisboa, Instituto Politécnico de Lisboa, Portugal

<sup>c</sup> CQE, IMS, DEQ, Instituto Superior Técnico, Universidade de Lisboa, Portugal

## ARTICLE INFO

### Article history:

Received 11 March 2022

Received in revised form

1 June 2022

Accepted 14 June 2022

Available online 27 June 2022

### Keywords:

Hybrid busbars

Galvanic corrosion

Destructive tests

Electrical resistance

Experimentation

## ABSTRACT

This paper is focused on the electrical and mechanical performance of aluminum-copper hybrid busbars subjected to corrosion over time. Two different types of hybrid busbars with joints produced by conventional fastening with M8 hexagonal socket head bolt-nut pairs made from medium carbon steel and by a new injection lap riveting process with semi-tubular rivets made from the material of the softer conductor are used and subjected to salt spray and electrochemical tests. Electrical resistance measurements performed on hybrid busbars taken from the corrosion testing cabinet at the end of each exposure period allow concluding that the new injection lap riveted hybrid busbars have a better electrical performance over time due to the elimination of fasteners with a higher electrical resistivity than aluminum and copper and to the elimination of the aluminum-steel and copper-steel galvanic pairs. The capability of the injection lap riveted hybrid busbars to withstand shear forces after corrosion testing also revealed to be adequate and like those of the original (uncorroded) hybrid busbars.

© 2022 The Authors. Publishing services by Elsevier B.V. on behalf of KeAi Communications Co. Ltd. This is an open access article under the CC BY-NC-ND license (<http://creativecommons.org/licenses/by-nc-nd/4.0/>).

## 1. Introduction

Switchgear systems, panel boards and busways make use of busbars to convey and distribute electrical power. Busbars are easy to install and maintain and are usually made of copper due to its high electrical conductivity, low coefficient of linear thermal expansion and resistance to corrosion.

However, the price of copper is extremely volatile and largely influenced by the global economy health due to its widespread utilization in electric power generation and transmission, and in other sectors of the economy related to transportation vehicles, machinery, electronics and building construction. In fact, the transition to a greener world built upon electric cars and power grids getting electricity from wind, solar and hydro sources is

surging the price of copper from roughly 5200 €/ton in January 2019 to a record high of 9300 €/ton in May 2021.

Given that fully electric cars on average require 80 kg of copper (i.e., four times more than internal combustion engine cars) [1], there is a growing interest in combining the electrical advantages of copper with the lightweight and economic advantages of aluminum (currently being traded at 2500 €/ton) by means of hybrid busbars. Hybrid busbars is a commonly used term to designate multi-material busbars, in which aluminum is the predominant material and copper is only used in the thinnest parts located at very specific locations.

The switch from copper to hybrid busbars comes at the risk of increasing the sensitivity to corrosion due to the contact between dissimilar materials and, therefore, at the expense of selecting (or developing) joining processes that minimize the effects of galvanic coupling without impairing the electrical and mechanical performances and increasing the overall complexity and cost of manufacturing. In fact, corrosion of the joints over time increases the electrical resistance, meaning that more power will be needed to distribute the current to the different components. For example, in electric cars this means more power required from the battery

\* Corresponding author.

E-mail addresses: [rui.f.sampaio@tecnico.ulisboa.pt](mailto:rui.f.sampaio@tecnico.ulisboa.pt) (R.F.V. Sampaio), [joao.pragana@tecnico.ulisboa.pt](mailto:joao.pragana@tecnico.ulisboa.pt) (J.P.M. Pragana), [ibraganca@dem.isel.ipl.pt](mailto:ibraganca@dem.isel.ipl.pt) (I.M.F. Bragança), [carlos.alves.silva@tecnico.ulisboa.pt](mailto:carlos.alves.silva@tecnico.ulisboa.pt) (C.M.A. Silva), [joao.salvador@tecnico.ulisboa.pt](mailto:joao.salvador@tecnico.ulisboa.pt) (J.C.S. Fernandes), [pmartins@tecnico.ulisboa.pt](mailto:pmartins@tecnico.ulisboa.pt) (P.A.F. Martins).

packs to the electric motors, electric transmission, electronic controllers, direct current converters, and other devices. In limiting conditions, the corroded joints begin to flake and fall apart compromising both the electrical and mechanical resistances.

The connection of copper and aluminum strips in hybrid busbars is commonly accomplished by the three main technologies that are schematically illustrated in Fig. 1.

The welding technology refers to a wide range of processes that include laser beam welding (Fig. 1a) [2], resistance spot welding [3] and ultrasonic welding [4], among others. Laser beam welding and resistance spot welding are used in electric cars for connecting battery cell terminals to monolithic busbars made from copper. However, their application in hybrid busbars made from aluminum and copper strips is constrained by changes in the mechanical properties of the heat-affected zones and by the formation of hard and brittle intermetallic compounds that influence both electrical and mechanical resistances [5]. Ultrasonic welding circumvents the above-mentioned limitations, but its application is limited to thin strips and may give rise to plastic deformation of the strip surfaces due to differences in the mechanical strengths of aluminum and copper.

Fastening (Fig. 1b) is the most widespread technology to connect monolithic busbars. Their use in hybrid busbars is encouraged by the ease of assembling and disassembling during installation, maintenance, and removal of the aluminum and copper strips at the end of service life. The main disadvantages of fastening are the distortion of the electric current flow in the joints and the high sensitivity to corrosion. The distortion of the electric current flow results from the non-uniform contact pressures, the condition of the surfaces and the unintentional self-loosening of the fasteners [6]. The high sensitivity to corrosion is due to the existence of three galvanic pairs (aluminum-copper, aluminum-steel, and copper-steel) and to the configuration and internal stresses at the joints, so that galvanic corrosion may occur, as well as crevice corrosion and stress corrosion cracking [7].

Joining by forming technology is also utilized to connect aluminum and copper strips in hybrid busbars. Processes involving the use of auxiliary elements such as self-pierce riveting [8] (Fig. 1c (left)) and self-clinching [9] avoid the thermal and metallurgical difficulties of welding but are sensitive to the effect of galvanic coupling. In fact, they are as sensitive to galvanic coupling as fastening because the auxiliary elements are usually made of steel.

One solution to reduce the number of galvanic pairs and, therefore, to reduce the effect of galvanic coupling is to connect the aluminum and copper strips by clinching [10] (Fig. 1c (right)), because no rivets or other types of auxiliary elements are used.

However, the process is only feasible for the connection of thin strips with good formability to prevent failure by cracking and the resulting joints are only capable of withstanding very small torques.

A solution that seeks to combine the main advantages of joining by forming with and without auxiliary elements was recently presented by Ferreira et al. [11], who developed a new process named ‘injection lap riveting’ (ILR) that uses auxiliary elements (semi-tubular rivets) made from the softer material of the two strips to be joined. In their work, Ferreira et al. [11] were mainly focused on the guidelines for dimensioning the cross sections of the aluminum and copper strips and for selecting the most appropriate geometry for the semi-tubular rivets taking into consideration their intended utilization. The electrical and mechanical performances of the resulting hybrid busbars were evaluated, but no studies were performed on the influence of corrosion on these performances over time.

Under these circumstances, the main objective of this paper is to evaluate and compare the electrical and mechanical resistances of fastened and injection lap riveted hybrid busbars subjected to corrosion. This is important to determine whether corrosion resistance of the injection lap riveted hybrid busbars adds to the advantages regarding the elimination of strip thickness limitations and protrusions above and below the strip surfaces that were previously identified by the authors [11].

For this purpose, authors prepared a set of fastened and injection lap riveted samples that are representative of the hybrid busbars, subjected the samples to salt spray tests and determined the evolution of the electrical resistance over time. The samples were also subjected to shear destructive forces before and after corrosion tests.

## 2. Materials and methods

### 2.1. Materials

The conductors of the hybrid busbars were made from AA6082-T6 aluminum and C11000 copper strips. M8 hexagonal socket head bolt-nut pairs made from medium carbon steel (class 8.8) were utilized in the fastened joints whereas semi-tubular rivets made from C11000 copper were employed in the injection lap riveted joints.

The AA6082-T6 aluminum and C11000 copper strips were subjected to tensile tests. The tests were carried out in an Instron 4507 universal testing machine at ambient temperature and the specimens were extracted from the strips in accordance with the ASTM standards E8/E8M [12].

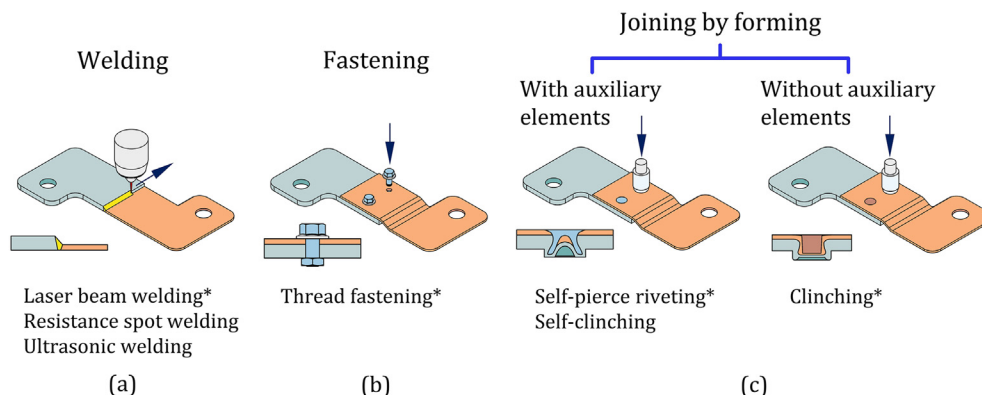


Fig. 1. Connection of aluminum and copper strips in hybrid busbars by means of (a) welding, (b) fastening and (c) joining by forming with details of the corresponding cross sections. The asterisk ‘\*’ refers the process shown in the top figure.

The electrical resistivities of the AA6082-T6 aluminum and C11000 copper strips were obtained in the experimental apparatus that will be introduced later in Section 2.3, when describing the procedure for determining the electrical resistance of the joints subjected to corrosion over time.

Table 1 presents a summary of the mechanical and electrical properties of the materials that were used in the fastened and injection lap riveted joints of the hybrid busbars. Data for medium carbon steel (class 8.8) was retrieved from literature [13,14].

## 2.2. Hybrid busbar specimens

Busbars are manufactured in a multitude of shapes and sizes depending on the geometric, electrical, and mechanical requirements of each application. In a previous work, Sampaio et al. [15] showed that the following relation between the cross-sectional ratio  $A_{Al}/A_{Cu}$  and the electrical resistivity ratio  $\rho_{Al}^e/\rho_{Cu}^e$  of the aluminum and copper strips must prevail to ensure equal electrical conductance  $G$  (i.e., equal current flow) in both strips,

$$G = \frac{A}{\rho^e l} \rightarrow \frac{A_{Al}}{A_{Cu}} = \frac{\rho_{Al}^e}{\rho_{Cu}^e} = 2.3 \quad (1)$$

where  $l$  is the length of the strips.

The present investigation used fastened and injection lap riveted hybrid busbar test specimens with a constant width  $w = 50$  mm and an overlapped length  $l_{ov} = 50$  mm made from aluminum strips with  $t_{Al} = 5$  mm thickness and  $l_{Al} = 100$  mm length, and copper strips with  $t_{Cu} = 2$  mm thickness and  $l_{Cu} = 100$  mm length (Fig. 2a). The cross-sectional ratio  $A_{Al}/A_{Cu} = 2.5$  of the test specimens resulting from the utilization of commercial strips available in the market is close to that required in (1) and the overall design gives emphasis to the joints in order to replicate the electric current flowing between the two conductors. This objective of using test specimens that replicate the electric current flow conditions in the conductors and joints, justifies the reason why they will be hereafter referred to as 'unit cells'.

The fastened unit cells were manufactured by drilling through holes of 8.4 mm diameter in the aluminum and copper strips, applying different surface preparations by mechanical grinding with emery paper of different grit sizes, and clamping the two strips together by application of different tightening torques  $T$  on the M8 hexagonal socket head bolts. The procedure is illustrated in Fig. 2b and the different fastened unit cells that were used in the investigation are summarized in Table 2.

The injection lap riveted unit cells were manufactured in a two-stage sequence (Fig. 2c). First, a dovetail ring hole (hereafter referred to as 'dovetail hole') and a countersunk hole are machined in the stronger and softer strips, respectively. Then a semi-tubular rivet made from the material of the softer strip is injected through the softer sheet into the dovetail hole of the stronger sheet to obtain the form-fit joint by mechanical interlocking.

Although injection lap riveting encompasses several parameters that are identified in Table 2 as: (i) the inclination angle  $\alpha$ , (ii) the

depth  $d_p$  and (iii) the thickness  $t$  of the dovetail holes, and (iv) the inner diameter  $d_i$ , (v) the outer diameter  $d_o$  and (vi) the shank length  $s$  of the rivets, this investigation was mainly focused on corrosion. Therefore, the experimental workplan made use of design values that were previously established by Ferreira et al. [11] and only varied the depth  $d_p$  and the shank length  $s$  of the rivets. Table 2 includes a summary of the two types of injection lap riveted unit cells that were used in the investigation.

## 2.3. Corrosion tests

Corrosion arising from interactions between the different materials of the unit cells was evaluated by means of: (i) salt spray (fog) tests and (ii) potentiodynamic polarization tests. Salt spray tests were carried out in a VLM corrosion testing cabinet type CCT 400-FL VDA-B under controlled temperature (35 °C), spraying a 3% sodium chloride (NaCl) solution with a flow rate of 0.26 L/h (Fig. 3a). The experimental procedure followed the ASTM B117 standard [16] for accelerated corrosion testing with periods of exposure of 6 h, 24 h, 48 h, 72 h, 120 h, etc ... until reaching the 30 days of total duration.

At the end of each period of exposure, a set of unit cells was taken from the cabinet and subjected to electrical resistance measurements, in accordance with the experimental methods and procedures that will be later described in the paper. Destructive shear tests were also performed on the unit cells after completion of the corrosion tests.

To prevent corrosion in the regions where the electric measurement probes are connected and the unit cells are fixed to the clamps of the universal testing machine, the non-overlapped regions of the aluminum and copper strips were covered with a 3 M™ Scotchrap™ all-weather corrosion protection tape (refer to Fig. 3a).

Potentiodynamic polarization tests employing a three-electrode configuration setup were utilized to understand the corrosion tendency of the different materials of the unit cells. Fig. 3b presents a scheme of the three-electrode configuration setup consisting of a Gamry 1010 E potentiostat, and a working electrode made from a material sample of the unit cells, a platinum coil as counter electrode (Pt) and a reference saturated calomel electrode (Hg/Hg<sub>2</sub>Cl<sub>2</sub>), immersed in a 3% NaCl solution.

The couple potential and the current flowing between each pair of materials of the unit cells (Cu–Al, Cu–Fe and Fe–Al) in natural conditions were also determined using a ZRA – zero resistance ammeter, in a configuration with two working electrodes (one of each element of the pair) and a saturated calomel electrode as reference. Additionally, the same procedure was followed with couples consisting in associations of the three materials (CuFe–Al, CuAl–Fe and FeAl–Cu), in which two of them were in contact, acting as one electrode, and the third was the second electrode. In all these measurements, the surface area of each material was chosen to replicate the area ratios in the unit cells.

The working electrodes were machined from the different materials of the unit cells to maintain their relative exposed areas, soldered to a copper wire, cleaned with acetone and ethanol, and

**Table 1**  
Summary of the mechanical and electrical properties of the materials.

	AA6082-T6 aluminum	C11000 copper	Steel (class 8.8)
Elastic modulus (GPa)	69	110	205
Poisson ratio	0.33	0.36	0.29
Yield strength (MPa)	260	222	640
Tensile strength (MPa)	309	300	800
Electrical resistivity ( $\mu\Omega\cdot m$ )	0.0361–0.0394	0.0170–0.0187	0.213

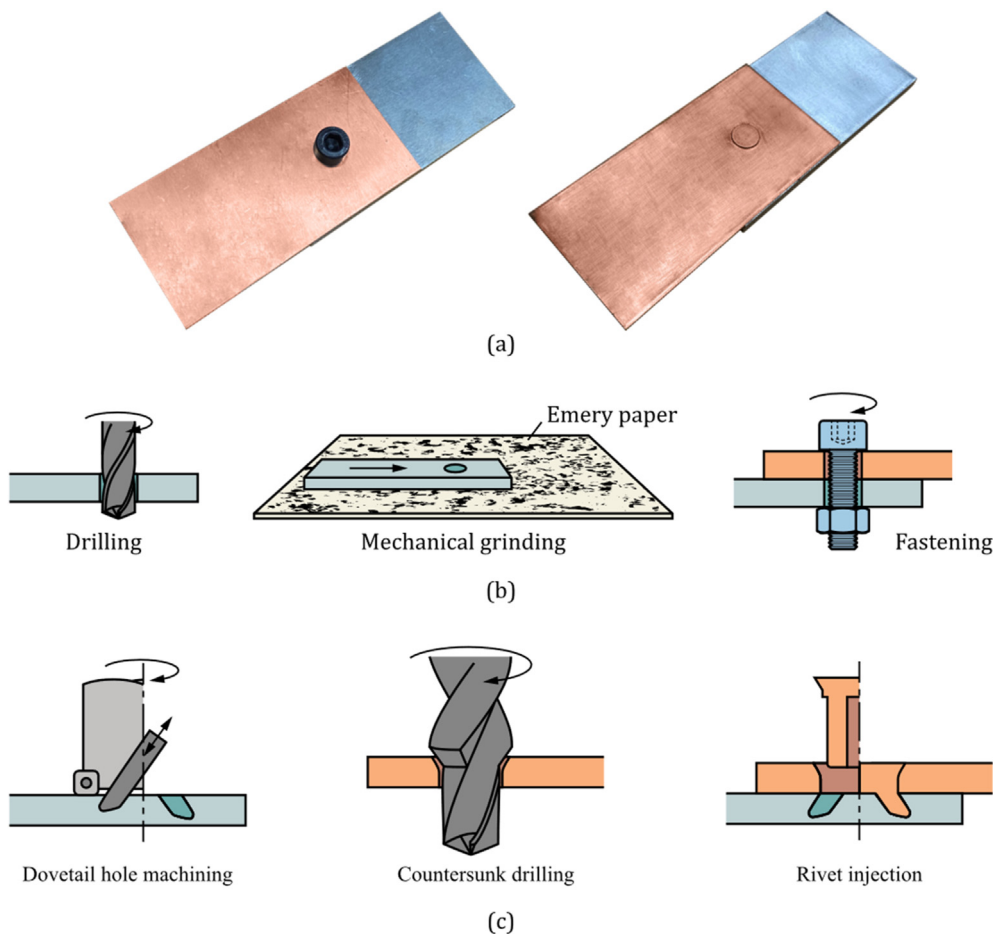
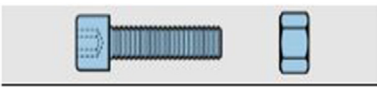
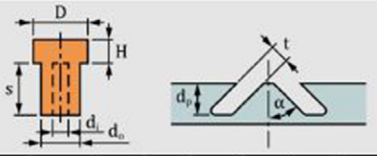


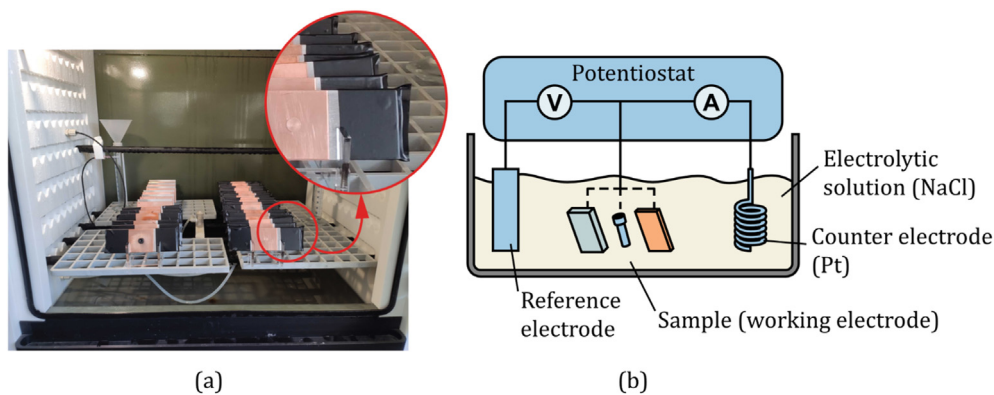
Fig. 2. Unit cells utilized for replicating the hybrid busbars, showing: (a) Fastened and injection lap riveted unit cells, (b) schematic representation of the procedure utilized to fabricate the fastened unit cells, (c) schematic representation of the procedure utilized to fabricate the injection lap riveted unit cells.

Table 2  
Summary of the materials and parameters of the fastened and injection lap riveted unit cells.

Strips	$l \times w \times t$ (mm <sup>3</sup> )							
AA6082-T6 aluminum	100 × 50 × 5							
C11000 copper	100 × 50 × 2							
<b>Fastener</b>								
Medium carbon steel (class 8.8)	<b>Size</b> M8							
Surface strip preparation	<b>Emery paper grit size</b> As supplied, 80, 1200							
Tightening torque (Nm)	<b>T (Nm)</b> 1, 5, 20							
<b>Semi-tubular rivet and strip</b>								
C11000 copper (semi-tubular rivet)	$d_i$ (mm)	$d_o$ (mm)	$D$ (mm)	$H$ (mm)	$s$ (mm)	$\alpha$ (°)	$d_p$ (mm)	$t$ (mm)
AA6082-T6 aluminum (strip)	2.0 ± 0.1	6.6 ± 0.1	10	2.2	4.9–6.9	30	3, 4	2.3 ± 0.1

subsequently dried and inserted into an epoxy casting mold. The polarization curves for the different materials of the unit cells are provided in the section ‘Results and discussion’ and were obtained

by establishing a steady-state open circuit for approximately 300 s to measure the corresponding potential and then ramping the applied potential at a scan rate of 1 mV/s in both the positive and



**Fig. 3.** Corrosion tests. (a) Photograph of the unit cells inside the corrosion testing cabinet where the salt spray tests were performed, showing a detail of the black corrosion protection tape applied on the non-overlapped surfaces of the aluminum and copper strips. (b) Schematic representation of the potentiodynamic polarization tests employing a three-electrode configuration setup.

negative directions (for the anodic curves and cathodic curves, respectively) while continuously measuring the electric current until a maximum of 5 mA.

**2.4. Electrical resistance and shear destructive tests**

The electrical resistance of the unit cells was measured in an experimental setup consisting of two copper blocks, where the unit cell ends taken from the corrosion testing cabinet at the end of each exposure period were clamped and connected to the power supply of a micro-ohmmeter KoCoS PROMET R600 (Fig. 4a). A current of 600 A passed through the unit cells during approximately 2 s to allow measuring the voltage drop *V* between two probes spaced 100 mm apart and calculating the electrical resistance from Ohm's law.

Thermal images were recorded with an infrared camera FLIR E86 (Flir Systems) equipped with a focal plane array microbolometer detector having 464 × 348 resolution and spectral range of 7.5–14 μm for attaining thermal imaging distributions on corroded and uncorroded unit cells. The absolute accuracy of the measurements is of ±2 °C (2% of reading) and the thermal sensitivity is lower than 40 mK at 30 °C.

The influence of corrosion on the maximum shear force that the unit cells can withstand was determined by subjecting samples after completion of the salt spray tests to destructive shear tests in the Instron 4507 universal testing machine that had been previously used in the mechanical characterization of the strip materials.

The tests were performed at ambient temperature with a crosshead speed of 5 mm/min and results were compared with those obtained from the original (uncorroded) unit cells. A schematic detail of the experimental setup is provided in Fig. 4b.

**3. Results and discussion**

**3.1. Corrosion of the unit cells**

Fig. 5a presents the anodic and cathodic polarization curves (potential as a function of the cathodic and anodic currents) obtained from the potentiodynamic polarization tests with a three-electrode configuration setup for the three different materials that were utilized in the investigation.

In these curves, the anodic processes, occurring at potentials higher than the open circuit potential, correspond to the oxidation of each metal, whereas the cathodic processes are normally reductions of species of the surrounding environment, in particular the reduction of water with release of hydrogen gas or the reduction of dissolved oxygen. By overlapping the curves from two different materials it is possible to predict the galvanic corrosion behavior of the couple. The intersection of the anodic curve of the less noble material with the cathodic curve of the most noble one gives an indication of the expected couple natural potential and of the current flowing between them. The less noble material will dissolve, being corroded, whereas the most noble will remain protected.

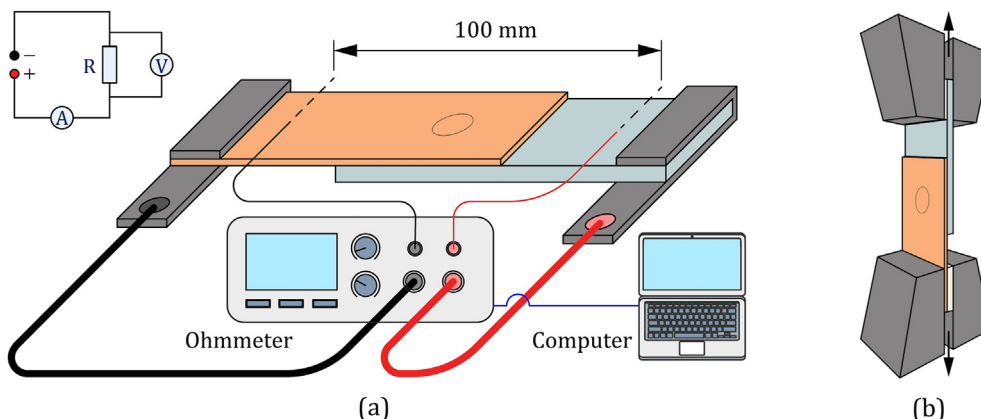


**Fig. 4.** Schematic representation of the (a) electrical resistance and (b) shear destructive tests performed on the unit cells.



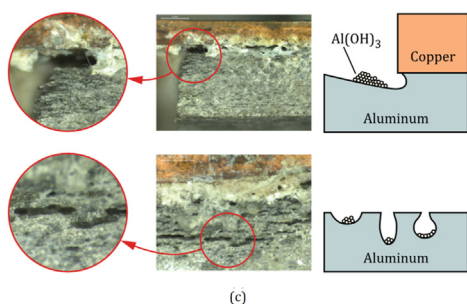
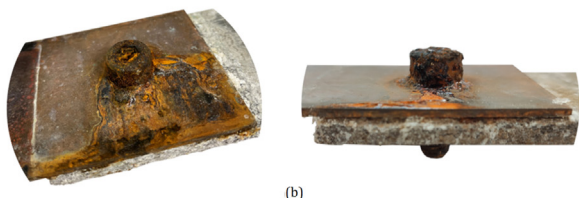
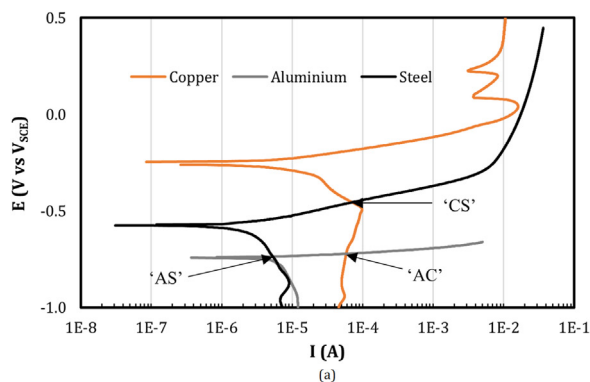


**Fig. 5.** Corrosion of the unit cells showing: (a) Polarization curves of aluminum AA6082-T6, C11000 copper and medium carbon steel (class 8.8) obtained from the potentiodynamic polarization tests with a three-electrode configuration setup, (b) photographic detail of a fastened unit cell after subjection to salt spray corrosion test, (c) schematic and photographic details of galvanic corrosion and corrosion by pitting of the aluminum strips in the fastened and injection lap riveted unit cells.

The relative order of the corrosion potentials and, therefore, the relative position of the polarization curves of each the different materials may be seen as the reason why the hexagonal socket head bolts in contact with the copper strips show higher material dissolution due to corrosion than the hexagonal nuts in contact with the aluminum strips (Fig. 5b). In fact, the steel bolts are less noble than copper and, in this way, they will corrode preferentially. On the contrary, the less noble aluminum part in the contact with the hexagonal nuts will corrode preferentially, protecting the nuts, where only cathodic reactions are expected to take place.

As seen, the intersections between the polarization curves of aluminum AA6082-T6 and medium carbon steel (refer to point 'AS' in Fig. 5a), aluminum AA6082-T6 and C11000 copper (point 'AC') and C11000 copper and medium carbon steel (point 'CS') indicate larger corrosion currents for the copper-steel galvanic pair with values close to those of the aluminum-copper pair. The aluminum-steel galvanic pair presents the smallest corrosion current with values about one order of magnitude smaller than the other pairs. This is an effect of the cathodic behavior of copper and steel, with steel showing currents one order of magnitude lower than copper.

Moreover, the near flat evolution of the anodic current of aluminum AA6082-T6 that is shown in Fig. 5a is typical of a passive material undergoing corrosion by pitting. This type of corrosion initiates at second phase particles or grain boundaries of the

aluminum strip surface and propagates along the thickness over time (Fig. 5c). The white colored regions on the contact interface between the aluminum and copper strips are due to galvanic corrosion with formation of aluminum hydroxide  $Al(OH)_3$  from the chemical reaction between aluminum and the water of the NaCl solution. Several forms of aluminum oxide/hydroxide can be considered. However, according to Pourbaix [17], the initial form of solid aluminum oxide is normally an amorphous hydroxide gel, corresponding practically to the composition  $Al(OH)_3$  and amphoteric in nature. However, this hydroxide gel is not stable, tending to crystallize to give first the monohydrate  $\gamma-Al_2O_3 \cdot H_2O$  (böhmite), later the trihydrate  $Al_2O_3 \cdot 3H_2O$  (bayerite) and finally another trihydrate, hydrargillite, in a process known as ageing. In the very aggressive and wet conditions of the salt spray test, the formation of aluminum hydroxide is expected to be the first step and, indeed, the formation of a gel is observed, no matter the future evolution of this product.

The occurrence of intergranular corrosion [18] and crevice corrosion of aluminum cannot also be discarded, due to the formation of intermetallic compounds and to the geometry of the unit cell which makes it prone to the second type of corrosion.

Fig. 6 presents the potential and current evolution with time for the ZRA tests in which two electrodes are made from material samples of the unit cells. The measurements of current over time confirm the lowest galvanic corrosion currents of the aluminum-steel galvanic pair, which keeps stable at a quite low current value within the duration of the test. In contrast, the other two galvanic pairs maintain higher galvanic currents, meaning that material dissolution will continue for longer durations of exposure. Moreover, the potentials  $V$  at the end of each test are compatible with those obtained for the intersection points 'AS', 'AC' and 'CS' of Fig. 5a.

Injection lap riveted unit cells lead to lower corrosion rate of aluminum due to the removal of one of the cathodic materials, steel. However, the elimination of the aluminum-steel galvanic pair has little relevance from a galvanic corrosion point of view due to the low cathodic current of steel.

To further understand the behavior of the systems with three metals in contact, the previous tests were repeated with couples consisting in associations of the three materials (CuFe–Al, CuAl–Fe and FeAl–Cu), in which two of them were in contact, as mentioned above. Fig. 7 presents the potential and current evolution with time for these tests.

To understand these results, it is important to define the polarity of the current values obtained, based on the designation of the system: a positive value corresponds to electrons flowing from the pair on the left to the metal on the right, so the former will be oxidized while reductions will take place on the later. In this frame, the negative current values of the system CuFe–Al indicate that electrons are flowing from Al to CuFe, so that aluminum is being oxidized whereas the couple CuFe is being protected from corrosion.

In the case of CuAl–Fe, the current is positive, so the flow of electrons is taking place from CuAl to Fe, with overall oxidation occurring on the CuAl couple and reductions taking place on Fe. However, from the result with only two materials, Cu is not expected to oxidize, so the anodic behavior is due to Al, meaning that both Cu and Fe are being protected on the expenses of Al corrosion. This also explains why the current values are, in this case, one order of magnitude lower than for the other systems, as most of the electron flow is occurring within the CuAl pair. Finally, in the case of FeAl–Cu the current is positive, so electrons are flowing from FeAl to Cu. Again, based on the previous results, Fe is expected to be protected in association with Al, so Al should be oxidized and both Fe and Cu are protected.

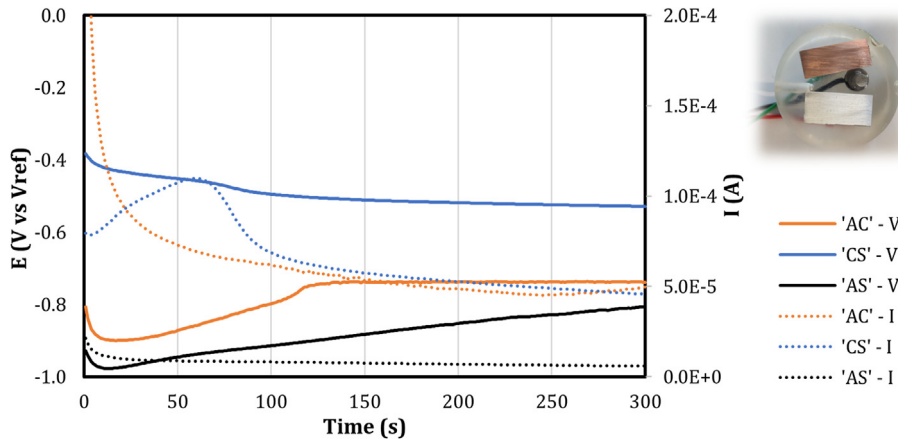


Fig. 6. Potential and current evolution with time for the ZRA tests in which two electrodes are made from material samples of the unit cells.

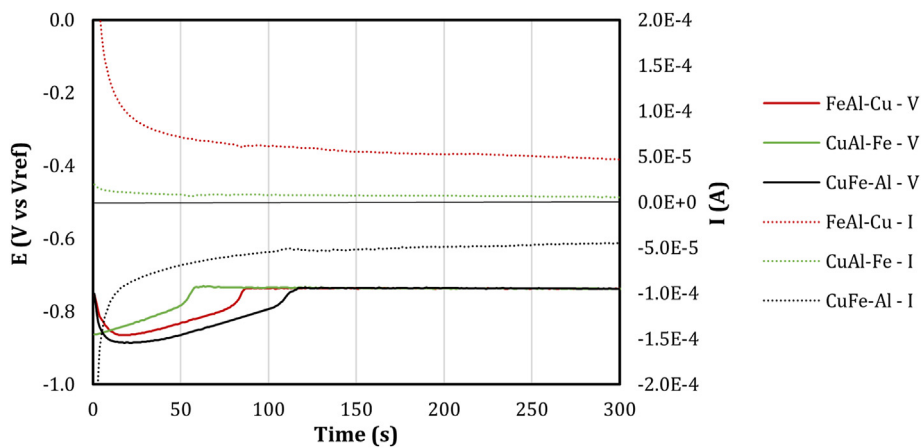


Fig. 7. Potential and current evolution with time for the ZRA tests with associations of the three materials.

The evolution of the natural potential of the systems confirms the above conclusions, as in all cases the potential tends to a value characteristic of Al corrosion ( $-738$  mV for CuFe–Al,  $-739$  mV for CuAl–Fe and  $-738$  mV for FeAl–Cu) and lower than the corrosion potentials of both Cu and Fe. So, in all cases the material corroding should be aluminum, therefore protecting both steel and copper.

### 3.2. Electrical resistance

Fig. 8 shows the evolution of the electrical resistance over time for the fastened and injection lap riveted unit cells subjected to salt spray corrosion tests. The surface of the fastened unit cells was ground with emery paper of 80 grit size whereas that of the

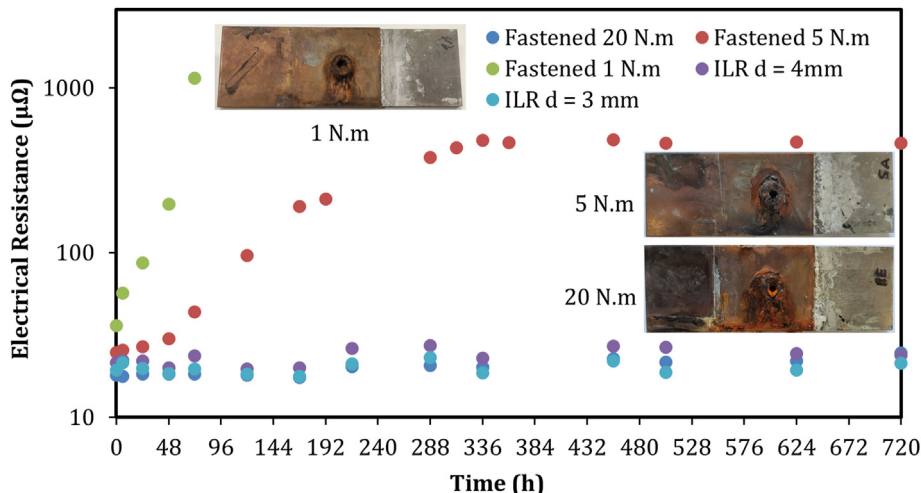


Fig. 8. Evolution of the electrical resistance with time for the fastened and injected lap riveted unit cells subjected to salt spray tests.

injected lap riveted unit cells was used as supplied (i.e., without surface preparation).

As seen, there are differences in the results obtained for the two types of unit cells because while the fastened unit cells show electrical resistance values that may vary over time up to two orders of magnitude, the injection lap riveted unit cells give values that only experience a minor increase over time.

The largest variation in electrical resistance occurs for the fastened unit cells with a loose clamping force resulting from a small tightening torque  $T = 1$  Nm (Table 3) due to easier access of the NaCl solution to the interface between the aluminum and copper strips. This facilitates galvanic corrosion with dissolution of aluminum and precipitation of aluminum hydroxide  $Al(OH)_3$ . The ingress of the aggressive medium that becomes trapped between the two surfaces with limited oxygen renovation, is also expected to create conditions prone to crevice corrosion.

Galvanic corrosion and precipitation of aluminum hydroxide  $Al(OH)_3$  with electrical insulation characteristics reduce the effective contact area between the two adjoining strips and, therefore, increase its electrical resistance to values above  $1000 \mu\Omega$ .

In connection to the above explanation, it is worth mentioning that the passage of electric current through the hexagonal socket head bolts and nuts is not relevant for the overall performance of the fastened unit cells due to the high electrical resistivity of steel [15]. In fact, the stabilization of electrical resistance around  $480 \mu\Omega$  for the fastened unit cells with a tightening torque of  $T = 5$  Nm is probably due to electric current flowing mainly through the hexagonal socket head bolts and nuts.

The smallest variation in the electrical resistance over time is observed for the fastened unit cells with larger tightening torques ( $T = 20$  Nm) and stronger clamping forces ( $F = 12.5$  kN in accordance with Table 3). In fact, values rise from approximately  $18 \mu\Omega$  to  $25 \mu\Omega$  during the entire duration of the corrosion tests, in close agreement with the results and growth rates found for the injection lap riveted unit cells ( $19 \mu\Omega$  to  $21 \mu\Omega$  for the semi-tubular rivet with a depth  $d_p = 3$  mm, and  $22 \mu\Omega$  to  $24 \mu\Omega$  for the semi-tubular rivet with a depth  $d_p = 4$  mm). The small variations in the electrical resistance that were measured for all these unit cells are attributed to the large pressures acting on the contact interfaces between the aluminum and copper strips because they prevent the aggressive solution to enter and the aluminum to dissolve and form aluminum hydroxide  $Al(OH)_3$ .

Thus, although dissolution and precipitation of aluminum hydroxide  $Al(OH)_3$  will occur along most of the contact interface between the aluminum and copper strips, it will not occur in the regions where the contact pressure is very high and where most of the electric current will flow because of the inverse proportionality between the electric contact resistivity  $\rho_c^e$  and the square root of the applied normal pressure  $p_n$  [19],

$$\rho_c^e = \frac{C}{\sqrt{p_n}} \tag{2}$$

In the above equation, C is a constant that depends on the sheet materials and temperature.

**Table 3**  
Tightening torques and analytical predicted clamping forces applied to the M8 hexagonal socket head bolts.

Torque $T$ (Nm)	Analytical force (kN)
1	0.625
5	3.125
20	12.5

The results shown in Fig. 9 allow understanding the influence of surface preparation on the evolution of electrical resistance with time for fastened unit cells subjected to salt spray tests. In fact, because the clamping force resulting from the tightening torque ( $T = 20$  Nm) is very strong, the influence of corrosion during the test duration is not as important as the surface preparation condition of the strip surfaces.

An increase in electrical resistance of approximately 20% is observed when the strips were utilized in the as supplied condition instead of being ground with emery paper of 80 grit size due to absence of cleaning and breaking of the contaminant and oxide films into small particles across the strip surfaces before tightening the aluminum and copper strips together.

Comparing the results obtained in Fig. 9 with those obtained for the injection lap riveted unit cells given in Fig. 8 allows concluding on the advantages of the latter because it has electrical resistances like those of the best fastened unit cells, with no surface preparation and no risk of unintentional self-loosening due to differences in temperature and/or applied forces leading to shifting of the clamped contact strip surfaces.

The importance of having regions where the contact pressure is very high to prevent the NaCl solution to enter and dissolve the aluminum with formation of aluminum hydroxide  $Al(OH)_3$ , is further proved in Fig. 9. In fact, by comparing the evolution of the electrical resistance over time of the fastened unit cells originally clamped with a tightening torque ( $T = 20$  Nm) with that of the fastened unit cells clamped with the same tightening torque after subjecting the individual strips to salt spray tests over different amounts of time, one concludes that the latter show values of approximately two orders of magnitude greater. This is attributed to the absence of uncorroded regions around the fasteners to facilitate the flow of electric current.

However, despite the influence of corrosion on the evolution of electrical resistance over time being small in case of the fastened unit cells subjected to a strong tightening torque ( $T = 20$  Nm), the increase in electrical resistance is still big enough for the temperature of a corroded joint to increase faster than that of an uncorroded joint, as it is shown in the thermal imaging distributions that are included in Fig. 10. The threshold temperature of  $105^\circ C$  was chosen in accordance with standards used for metal-clad switch-gears [20].

### 3.3. Destructive tests

The results of the destructive shear tests performed in the fastened and injection lap riveted unit cells before and after subjecting the unit cells to salt spray tests for 30 days are included in

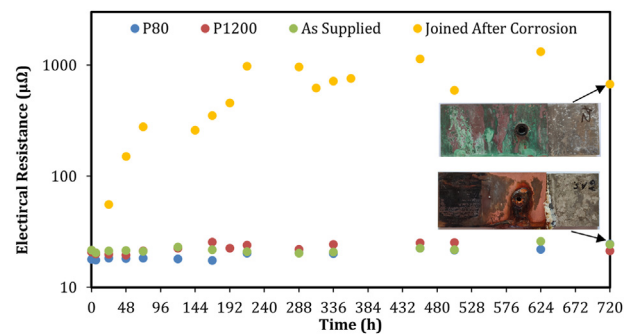


**Fig. 9.** Evolution of the electrical resistance with time for fastened unit cells ( $T = 20$  Nm) subjected to salt spray tests. The three series correspond to preliminary surface ground with emery paper of different grit sizes.



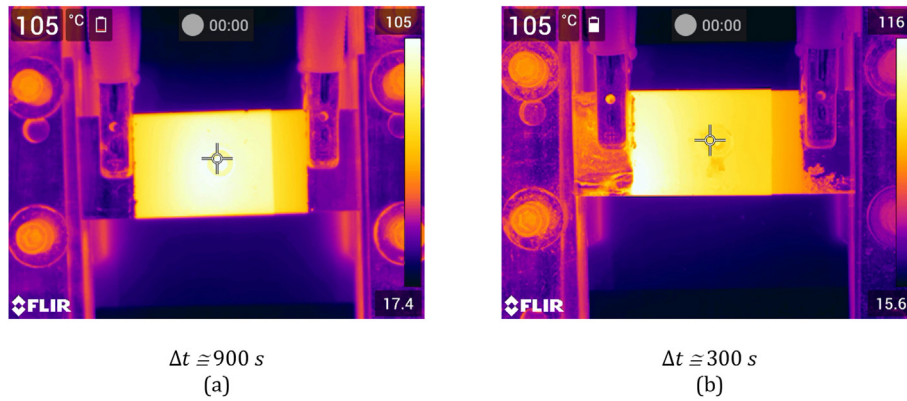


Fig. 10. Distribution of temperature for (a) uncorroded and (b) corroded fastened ( $T = 20 \text{ Nm}$ ) unit cells subjected to a current of 600 A with indication of the amount of time  $\Delta t$  needed to reach a maximum temperature of 105 °C at the center of the overlapped region.

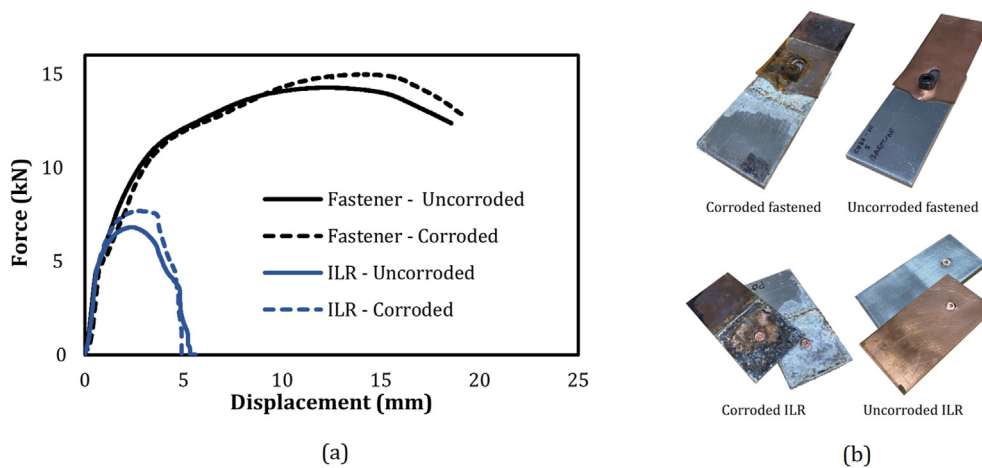


Fig. 11. (a) Destruction shear force vs. displacement for uncorroded and (b) corroded unit cells of fastened ( $T = 20 \text{ Nm}$ ) and injection lap riveted hybrid busbars.

Contrary to what one might initially expect, there are no significant differences between the peak forces and the force vs. displacement evolutions obtained for the non-corroded and corroded samples of each type of joint.

The slight increase in the shear mechanical strength of the corroded injection lap riveted joint against that of the uncorroded joint is attributed to minor additional artificial tightening of the semi tubular copper rivet caused by the aluminum hydroxide  $\text{Al}(\text{OH})_3$ , but the differences at the peak force values are smaller than 10%.

The better overall shear performance of the fastened joints is due to the utilization of M8 hexagonal socket head bolt-nut pairs made from medium carbon steel instead of semi-tubular rivets made from softer C11000 copper, as in case of the injection lap riveted joints. However, the performance of the latter is good enough for electric busbar applications, meaning that its advantage stem for the capability of providing electrical resistances like those of the best fastened unit cells, with no surface preparation and no risk of unintentional self-loosening.

#### 4. Conclusions

The main conclusions that can be drawn from this investigation on the influence of corrosion on the electrical and mechanical performance of hybrid busbars are the following:

- Fastened hybrid busbars with loose clamping forces subjected to salt spray tests allow the NaCl solution to penetrate into the contact interface between the conductors and dissolve the aluminum and form aluminum hydroxide  $\text{Al}(\text{OH})_3$ ;
- The dissolution of aluminum and formation of aluminum hydroxide  $\text{Al}(\text{OH})_3$  by galvanic corrosion increases the electrical resistance to values approximately two orders of magnitude higher than the hybrid busbars not exposed to corrosion;
- Fastened hybrid busbars with strong clamping forces subjected to salt spray tests do not allow the NaCl solution to penetrate the contact interface between the two conductors where most of the electric current flows, explaining the reason why the electrical resistance only increases by approximately 40% after 30 days of exposure to accelerated corrosion;
- Electrochemical tests performed on copper, steel, and aluminum unit cell materials allow concluding that aluminum will preferentially corrode and, therefore, will protect the other two materials from corrosion;
- The new injection lap riveted busbars are the least prone to corrosion with an increase in the electrical resistance of only 10% after 30 days of exposure to accelerated corrosion due to elimination of the steel cathodic surface area by using a semi-tubular copper rivet;
- Shear destructive tests with injection lap riveted busbars provide peak values that are appropriate for industrial applications involving passage and distribution of electrical power.

## Conflicts of interest

The authors declare that there is no conflicts of interest.

## Acknowledgments

The authors would like to acknowledge the support provided by Fundação para a Ciência e a Tecnologia of Portugal and IDMEC under LAETA- UIDB/50022/2020 and PTDC/EME-EME/0949/2020. CQE and IMS are financed by FCT under contracts UIDB/00100/2020 and UIDP/00100/2020 and LA/P/0056/2020.

## References

- [1] <https://www.mining.com/ev-sector-will-need-250-more-copper-by-2030-just-for-charging-stations/>.
- [2] S. Katayama, Introduction: fundamentals of laser welding, in: S. Katayama (Ed.), *Handbook of Laser Welding Technologies*, vols. 3–16, Woodhead Publishing, Cambridge, 2013.
- [3] M.J. Brand, A.S. Philipp, F.Z. Michael, J. Andreas, Welding techniques for battery cells and resulting electrical contact resistances, *J. Energy Storage* 1 (2015) 7–14, <https://doi.org/10.1016/j.est.2015.04.001>.
- [4] M.P. Matheny, K.F. Graff, Ultrasonic welding of metals, in: J.G. Juarez, K. Graff (Eds.), *Power Ultrasonics: Applications of High-Intensity Ultrasound*, Woodhead Publishing, Cambridge, 2015, pp. 259–293, <https://doi.org/10.1016/B978-1-78242-028-6.00011-9>.
- [5] P.A. Schmidt, M. Schweier, M.F. Zaeh, Joining of lithium-ion batteries using laser beam welding: electrical losses of welded aluminum and copper joints, *Proceedings of ICALEO - International Congress on Applications of Lasers & Electro-Optics* 31 (2012) 915–923, <https://doi.org/10.2351/1.5062563>.
- [6] R. Tzeneva, Y. Slavtchev, V. Mladenov, New connection design of high power bolted busbar connections, in: *Proceedings of the 11th WSEAS International Conference on Circuits, Greece, 2007*, pp. 228–233.
- [7] L. Calabrese, E. Proverbio, E. Pollicino, G. Galtieri, C. Borsellino, Effect of galvanic corrosion on durability of aluminium/steel self-piercing rivet joints, *Corrosion Eng. Sci. Technol.* 501 (2015) 10–17, <https://doi.org/10.1179/1743278214Y.0000000168>.
- [8] M.W. Danyo, Self-piercing riveting (SPR) in the automotive industry: an overview, in: A. Chrysanthou, X. Sun (Eds.), *Self-Piercing Riveting – Properties, Processes and Applications*, 171–180, Woodhead Publishing, Cambridge, 2014, <https://doi.org/10.1533/9780857098849.2.171>.
- [9] R.W. Messler, *Joining of Advanced Materials*, Butterworth-Heinemann, Boston, 1993.
- [10] U. Füssel, J. Kalich, Joining by forming-solutions for multi material design, in: *Proceedings of the 9th International Conference on Advances in Resistance Welding Florida, USA, 2016*.
- [11] F.R. Ferreira, J.P.M. Pragana, I.M.F. Bragança, C.M.A. Silva, P.A.F. Martins, Injection lap riveting, *CIRP Ann. - Manuf. Technol.* 70 (2021) 261–264.
- [12] ASTM E8/E8M, *Standard Test Methods for Tension Testing of Metallic Materials*, ASTM International, West Conshohocken, PA, USA, 2016.
- [13] ISO 898-1:2013, *Mechanical Properties of Fasteners Made of Carbon Steel and Alloy Steel - Part 1: Bolts, Screws and Studs with Specified Property Classes - Coarse Thread and Fine Pitch Thread*, International Organization for Standardization ISO Geneva, Switzerland, 2013.
- [14] ISO 898-2:2012, *Mechanical Properties of Fasteners Made of Carbon Steel and Alloy Steel - Part 2: Nuts with Specified Property Classes - Coarse Thread and Fine Pitch Thread*, International Organization for Standardization ISO Geneva, Switzerland, 2012.
- [15] R.F.V. Sampaio, J.P.M. Pragana, I.M.F. Bragança, C.M.A. Silva, C.V. Nielsen, P.A.F. Martins, Electric performance of fastened hybrid busbars: an experimental and numerical study, *J. Mater. Design Appl.* 236 (6) (2022) 1152–1163.
- [16] ASTM B117-19, *Standard Practice for Operating Salt Spray (Fog) Apparatus*, ASTM International, West Conshohocken, PA, USA, 2019.
- [17] M. Pourbaix, *Atlas of Electrochemical Equilibria in Aqueous Solutions*, NACE - National Association of Corrosion Engineers, Houston, 1974.
- [18] Y. Xie, X. Meng, F. Wang, Y. Jiang, X. Ma, L. Wan, Y. Huang, Insight on corrosion behavior of friction stir welded AA2219/AA2195 joints in astronautical engineering, *Corrosion Sci.* 192 (2021), 109800.
- [19] F.J. Studer, Contact resistance in spot welding, *Weld. J.* 18 (1939) 374–380.
- [20] C37.20.2-2015, in: *IEEE Standard for Metal-Clad Switchgear*, IEEE Standards Association, Piscataway, NJ, USA, 2015.